Ultimate quantum limit for amplification: A single atom in front of a mirror

New Journal of Physics
The open access journal at the forefront of physics

Deutsche Physikalische Gesellschaft DPG
IOP Institute of Physics

Published in partnership with: Deutsche Physikalische Gesellschaft and the Institute of Physics

OPEN ACCESS

RECEIVED
23 December 2020

REVISED
19 March 2021

ACCEPTED FOR PUBLICATION
24 March 2021

PUBLISHED
20 May 2021

PAPER

Ultimate quantum limit for amplification: a single atom in front of a mirror

Emely Wiegand[1,*], Ping-Yi Wen[2], Per Delsing[1], Io-Chun Hoi[3,4] and Anton Frisk Kockum[1,*]

[1] Department of Microtechnology and Nanoscience (MC2), Chalmers University of Technology, 412 96 Gothenburg, Sweden
[2] Department of Physics, National Chung Cheng University, Chiayi 621301, Taiwan
[3] Department of Physics, National Tsing Hua University, Hsinchu 30013, Taiwan
[4] Center for Quantum Technology, National Tsing Hua University, Hsinchu 30013, Taiwan
[*] Authors to whom any correspondence should be addressed.

E-mail: wiegand@chalmers.se and anton.frisk.kockum@chalmers.se

Keywords: quantum optics, waveguide quantum electrodynamics, circuit quantum electrodynamics, quantum mechanics, amplification

Abstract

We investigate three types of amplification processes for light fields coupling to an atom near the end of a one-dimensional (1D) semi-infinite waveguide. We consider two setups where a drive creates population inversion in the bare or dressed basis of a three-level atom and one setup where the amplification is due to higher-order processes in a driven two-level atom. In all cases, the end of the waveguide acts as a mirror for the light. We find that this enhances the amplification in two ways compared to the same setups in an open waveguide. Firstly, the mirror forces all output from the atom to travel in one direction instead of being split up into two output channels. Secondly, interference due to the mirror enables tuning of the ratio of relaxation rates for different transitions in the atom to increase population inversion. We quantify the enhancement in amplification due to these factors and show that it can be demonstrated for standard parameters in experiments with superconducting quantum circuits.

1. Introduction

Amplification of measurement signals is crucial to achieve good signal-to-noise ratios in many experiments in quantum information and quantum optics [1, 2]. Ideally, amplifiers used for such tasks should be compact, add as little noise as possible [3, 4], and produce high gain. To reach the ultimate limit in terms of size, a single atom or other quantum emitter could be used as an amplifier. However, to achieve high gain with a single quantum emitter coupled to an electromagnetic field in free space is extremely challenging, since imperfect spatial mode matching leads to a weak coupling [5–11]. The mode matching, and thus a strong coupling, is much easier to achieve when the propagation of the field is confined to a one-dimensional (1D) waveguide. Such systems are widely studied in waveguide quantum electrodynamics (waveguide QED), which has proven an excellent platform for quantum-optical experiments [12, 13].

In the past two decades, many quantum-optics phenomena have been demonstrated using superconducting circuits [13–16], e.g., lasing [17–20]. Superconducting circuits consist of superconducting qubits [15, 21] coupled to a coplanar waveguide (either open or made into a resonator) [13, 22–24] or three-dimensional cavities [13, 16, 25]. One advantage of superconducting circuits over natural atomic systems is that strong, and even ultrastrong, coupling between the quantum emitters and cavities or open waveguides can be achieved quite easily [26–32]. This advantage has, for example, been demonstrated by Wen *et al* [33], who used superconducting circuits to realize a 7% amplification of a weak probe signal on a strongly-driven two-level system coupled to a waveguide. Similar experiments with many natural atoms [34] or a single quantum dot [35] were only able to achieve 0.4% and 0.005% amplification, respectively.

The vast majority of waveguide-QED experiments with superconducting circuits so far were performed with one or more superconducting qubits coupled to an *open* waveguide [12, 13, 24, 29, 36–49]. However,

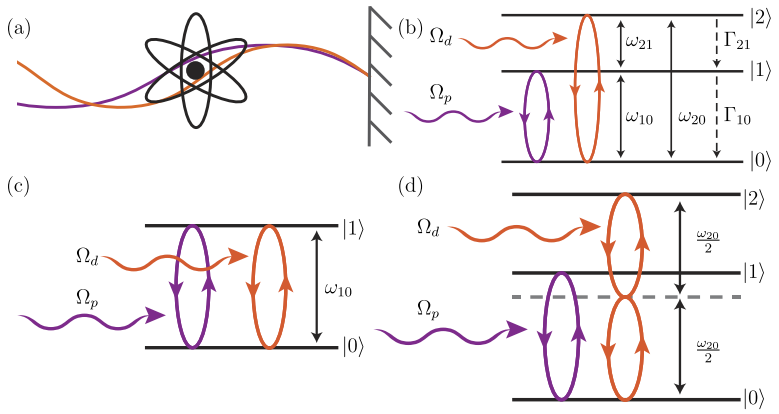

Figure 1. Sketches of the systems considered in this article. (a) All systems we study are variations on a setup with an atom in front of a mirror (short). The atom interacts with a strong drive field (orange) and a weak probe field (purple). (b) A three-level atom with transition frequencies ω_{ij} between the states $|i\rangle$ and $|j\rangle$. The atom is strongly driven with a drive amplitude Ω_d on the $|0\rangle \leftrightarrow |2\rangle$ transition. The probe field with amplitude Ω_p is applied to the $|0\rangle \leftrightarrow |1\rangle$ transition. The decay rates are denoted by Γ_{ij} for the transition from $|i\rangle$ to $|j\rangle$. (c) A two-level system both driven and probed around its transition frequency ω_{10}. (d) A three-level atom like in (b), but driven at half the frequency of the $|0\rangle \leftrightarrow |2\rangle$ transition, resulting in a two-photon driving that dresses all states of the weakly anharmonic system.

the waveguide can also be shorted or left open at one end, where an incoming electromagnetic field will be reflected with a phase shift [33, 50–52]. When a superconducting qubit is included [33, 52], this setup is equivalent to putting an atom in front of a *mirror*, which has been studied experimentally [33, 46, 52–57] and theoretically [58–70] for both natural and artificial atoms. In this article, we investigate the advantages of using an atom in front of a mirror, instead of an atom in an open waveguide, for signal amplification.

There are several ways to achieve amplification in an atomic system driven by an electromagnetic field. One amplification mechanism is population inversion, where excitations are pumped into higher atomic levels with a finite life time, where they stay long enough to induce amplification through stimulated emission [71, 72]. There are also mechanisms that can lead to amplification and lasing without inversion in the bare-state basis [73]. For instance, if an atom is driven strongly, the energy levels can split and population inversion can occur in the dressed-state basis [40, 74] if the drive is off resonance. If the drive is on resonance, the power spectrum exhibits the so-called Mollow triplet [24, 56, 75, 76]; amplification without population inversion can then be achieved at frequencies between the triplet peaks due to higher-order processes between the dressed states of the driven atom [33–35, 77, 78].

We study all three amplification mechanisms outlined above for an atom, with either two or three levels, coupled to a 1D waveguide terminated by a mirror (in the form of a short) at one end, as depicted in figure 1. We show that this setup has two advantages over the corresponding one in an open waveguide, leading to a doubling or more of the maximum amplification that we can achieve. Firstly, the mirror reflects the electromagnetic field such that we only have one input–output channel, which avoids losing half of the atomic output in one direction, as happens in an open waveguide. The second advantage of the mirror setup is that, due to interference effects, the coupling to the waveguide is set by the position of the atom and its transition frequency. This enables manipulation of the relative coupling strengths for different transitions in a three-level atom, either by changing the atomic frequency, which is possible in superconducting circuits [13–16], or by changing the distance from the atom to the mirror. We note that the coupling strengths can also be made frequency-dependent and tunable using giant atoms [48, 49, 79–91], which couple to the waveguide at multiple points, but if the giant atom is placed in an open waveguide, the problem of losing half the output remains. With a mirror, a single small atom is simpler to implement than a giant atom, but still sufficient to achieve the advantageous frequency-dependent coupling.

The first system we consider is shown in figure 1(b) and discussed in section 2. It is a three-level atom with a strong drive on the transition between the ground state $|0\rangle$ and the second excited state $|2\rangle$. When the decay rate from $|2\rangle$ to the first excited state $|1\rangle$ is larger than the decay rate from $|1\rangle$ to $|0\rangle$, a population inversion between $|1\rangle$ and $|0\rangle$ is created. This leads to amplification of a weak probe signal on the $|0\rangle \leftrightarrow |1\rangle$ transition. We find that with the mirror, a maximum amplitude gain of 25% can be reached, whereas the maximum amplification in an open waveguide is 12.5% [36].

Next, we study, in section 3, the resonantly driven two-level atom depicted in figure 1(c). The strong drive splits the energy levels of the atom and enable transitions in the dressed-state basis. By probing the system in the vicinity of the bare resonance frequency, we achieve a maximal amplitude gain of around 6.9% with the mirror. For an open waveguide, we find an amplification of around 3.4% for the same system

parameters. In contrast to the previous case, amplification is not due to population inversion, but enabled by higher-order processes between the dressed states [33, 78].

The last system we study, in section 4, is the three-level system shown in figure 1(d), driven at half the $|0\rangle \leftrightarrow |2\rangle$ transition frequency. Similarly to the strongly driven two-level system, the energy levels are split by the driving and transitions take place between dressed states. By probing the system, we find a maximal amplification of around 6.2% with a mirror, which exceeds the amplification of the same setup in an open waveguide by more than a factor 2 [40]. Here the amplification is due to hidden inversion—population inversion between the dressed states of the system.

We further show that all these systems can be realized with currently available state-of-the-art technology in experimental waveguide-QED setups with a transmon qubit [92] coupled to a 1D transmission line. The transition frequencies of such a qubit are tunable *in situ*, which means that the ratio of the decay rates of the transmon can be chosen to reach the optimal amplification settings. Our proposed setups, which represent an ultimate quantum limit for amplification, may thus find applications in superconducting quantum information processing.

2. Amplification with a strongly driven three-level atom in front of a mirror

We begin by studying the setup with a three-level atom in front of a mirror shown in figure 1(b). The system is coherently driven with amplitude Ω_d on the transition between the ground state $|0\rangle$ and the second excited state $|2\rangle$. The aim is to create a population inversion between the states $|0\rangle$ and $|1\rangle$, which can lead to a gain in the reflection of a weak coherent probe resonant with the $|0\rangle \leftrightarrow |1\rangle$ transition. To achieve population inversion, the life-time $1/\Gamma_{10}$ of the first excited state should be much longer than the life-time $1/\Gamma_{21}$ of the second excited state. Here, we assume that the atom is a good approximation of a ladder-type Ξ system with $\Gamma_{20} \ll \Gamma_{10}, \Gamma_{21}$.

2.1. Hamiltonian and master equation

The Hamiltonian of the system in the frame rotating at the drive frequencies is (we set $\hbar = 1$ throughout this article)

$$H = H_\mathrm{a} + H_\mathrm{int}, \tag{1}$$

$$H_\mathrm{a} = \delta\omega_{10}\sigma_{11} + \delta\omega_{20}\sigma_{22}, \tag{2}$$

$$H_\mathrm{int} = \frac{\Omega_\mathrm{d}}{2}\left(\sigma_{20} + \sigma_{02}\right) + \frac{\Omega_\mathrm{p}}{2}\left(\sigma_{10} + \sigma_{01}\right), \tag{3}$$

where $\sigma_{ij} = |i\rangle\langle j|$, the drive amplitude on the $|0\rangle \leftrightarrow |2\rangle$ ($|0\rangle \leftrightarrow |1\rangle$) transition is given by Ω_d (Ω_p), and $\delta\omega_{ij} = \omega_{ij} - \omega_{ij}^\mathrm{d}$ for $i > j$ is the detuning between the transition frequency $\omega_{ij} = \omega_i - \omega_j$ and the frequency ω_{ij}^d of the drive on that transition. The dynamics of the system is described by the master equation

$$\dot{\rho} = -\frac{i}{\hbar}\left[H, \rho\right] + \mathcal{L}\left[\rho\right] \tag{4}$$

for the density matrix $\rho = \sum_{i,j}\rho_{ij}|i\rangle\langle j|$. The Lindbladian term in equation (4) is given by

$$\mathcal{L}\left[\rho\right] = \Gamma_{21}\rho_{22}\left(-\sigma_{22} + \sigma_{11}\right) + \Gamma_{10}\rho_{11}\left(-\sigma_{11} + \sigma_{00}\right) - \sum_{i\neq j}\gamma_{ij}\rho_{ij}\sigma_{ij}, \tag{5}$$

with the dephasing $\gamma_{ij} = \gamma_{ji}$ and the relaxation rates Γ_{ij} between the states $|i\rangle$ and $|j\rangle$, $i > j$. Since we assume negligible temperature, we can neglect thermal excitations, i.e., $\Gamma_{01} = \Gamma_{12} = \Gamma_{02} = 0$.

2.2. Amplification and optimal drive strength in the steady state

We assume that the probe on the $|0\rangle \leftrightarrow |1\rangle$ transition is weak, i.e., $\Omega_\mathrm{p}/\Gamma_{10} \ll 1$, and that $\Gamma_{21} \gg \Gamma_{10}$ to ensure population inversion. Solving the master equation for the steady state ($\dot{\rho} = 0$), we obtain the following result for the reflection coefficient [36, 52, 56]

$$r = 1 - 2i\frac{\Gamma_{10}}{\Omega_\mathrm{p}}\langle\sigma_{01}\rangle = 1 + 2\Gamma_{10}\frac{(\rho_{11} - \rho_{00})}{2\lambda_{10} + \frac{\Omega_\mathrm{d}^2}{2\lambda_{12}}}, \tag{6}$$

where

$$\rho_{00} = \frac{\frac{2\Gamma_{21}|\lambda_{02}|^2}{\gamma_{20}\Omega_{20}^2} + 1}{\frac{2\Gamma_{21}|\lambda_{01}|^2}{\gamma_{20}\Omega_{20}^2} + \frac{\Gamma_{21}}{\Gamma_{10}} + 2} \qquad \rho_{11} = \frac{\frac{\Gamma_{21}}{\Gamma_{10}}}{\frac{2\Gamma_{21}|\lambda_{02}|^2}{\gamma_{20}\Omega_{20}^2} + \frac{\Gamma_{21}}{\Gamma_{10}} + 2} \tag{7}$$

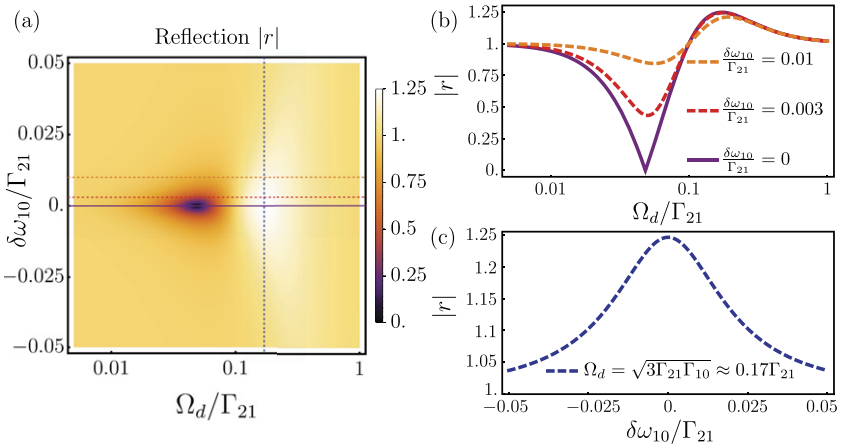

Figure 2. Optimizing the amplitude gain of a strongly driven three-level atom in front of a mirror. (a) The absolute value of the reflection coefficient, $|r|$, i.e., the amplitude gain, as a function of the drive strength Ω_d/Γ_{21} and the probe detuning $\delta\omega_{10}/\Gamma_{21}$. The reflection is calculated for a resonant drive, $\delta\omega_{20} = 0$, no pure dephasing, $\gamma_{21} = \gamma_{20} = \Gamma_{21}/2$ and $\gamma_{10} = \Gamma_{10}/2$, and with $\Gamma_{10}/\Gamma_{21} = 0.01$. The reflection reaches its maximum at $\Omega_{20} = \sqrt{3\Gamma_{21}\Gamma_{10}} \approx 0.17\Gamma_{21}$. (b) Horizontal linecuts from panel (a) showing the amplitude gain as a function of Ω_d for three different values of the probe detuning: $\delta\omega_{10} = 0$ (purple, solid curve), $\delta\omega_{10}/\Gamma_{21} = 0.003$ (red, dashed), and $\delta\omega_{10}/\Gamma_{21} = 0.01$ (orange, dashed). The maximum values for the orange and red curves are slightly below 1.25. (c) Vertical blue dashed linecut from panel (a) showing the reflection at the optimal driving strength $\Omega_d = \sqrt{3\Gamma_{21}\Gamma_{10}} \approx 0.17\Gamma_{21}$ as a function of the detuning $\delta\omega_{10}/\Gamma_{21}$.

and $\lambda_{ij} = \lambda_{ji}^*$ with

$$\lambda_{10} = \gamma_{10} + i\delta\omega_{10}, \qquad \lambda_{12} = \gamma_{21} - i\delta\omega_{20} + i\delta\omega_{10}, \qquad \lambda_{02} = \gamma_{20} - i\delta\omega_{20}. \tag{8}$$

More details of the derivation are given in appendix A. The reflection coefficient deviates from that in reference [36] for an open waveguide. The mirror adds a factor 2 to the second term of the reflection coefficient in equation (6) compared to the open waveguide, which leads to an enhancement of the gain, see figure 2.

From equation (6), it is clear that amplification requires $\rho_{11} > \rho_{00}$, which leads to

$$\Omega_d^2 > \frac{2\Gamma_{10}|\lambda_{02}|^2}{\gamma_{20}} + \frac{\Omega_d^2\Gamma_{10}}{\Gamma_{21}} \approx \frac{2\Gamma_{10}|\lambda_{02}|^2}{\gamma_{20}}. \tag{9}$$

For a resonant drive, $\delta\omega_{20} = 0$, and no pure dephasing, $\gamma_{20} = \Gamma_{21}/2$, this inequality reduces to

$$\Omega_d^2 > \Gamma_{10}\Gamma_{21}. \tag{10}$$

We now calculate the maximal possible amplitude gain of the single-atom amplifier. We consider double resonance, $\delta\omega_{20} = \delta\omega_{10} = 0$, and no pure dephasing, i.e., $\gamma_{10} = \Gamma_{10}/2$, $\gamma_{21} = \Gamma_{21}/2$, and $\gamma_{20} = \Gamma_{21}/2$. We find (see appendix A) that the reflections reaches its maximum value if the drive amplitude is given by

$$\Omega_d^2 = 3\Gamma_{10}\Gamma_{21}. \tag{11}$$

With this value, the maximum reflection is given by

$$|r| = 1 + \frac{1}{4}, \tag{12}$$

which corresponds to an amplitude gain of 25%. If we include higher orders of Γ_{10}/Γ_{21} in the calculation, the first-order correction to the maximum value of the reflection becomes

$$r = 1 + \frac{1}{4} - \frac{3}{8}\frac{\Gamma_{10}}{\Gamma_{21}} + \mathcal{O}\left(\frac{\Gamma_{10}}{\Gamma_{21}}\right)^2. \tag{13}$$

In figure 2(a), we plot the absolute value of the reflection coefficient as a function of the drive amplitude Ω_d and the detuning $\delta\omega_{10}$. In figure 2(b), we further illustrate the effect of non-zero detuning with a few linecuts from figure 2(a). It is clear that the maximum reflection is achieved on resonance.

2.3. Optimal population inversion

In the previous subsection, we found that the drive strength $\Omega_d^2 = 3\Gamma_{10}\Gamma_{21}$ gives the highest amplitude gain. Inserting this into the expressions for ρ_{00} and ρ_{11} in equation (7), we obtain

$$\rho_{00} = \frac{1}{\frac{4}{3} + 2\underbrace{\frac{\Gamma_{10}}{\Gamma_{21}}}_{\ll 1}} \approx \frac{3}{4}, \qquad \rho_{11} = \frac{\frac{1}{3} + \frac{\Gamma_{10}}{\Gamma_{21}}}{\frac{4}{3} + 2\frac{\Gamma_{10}}{\Gamma_{21}}} \approx \frac{1}{4}. \tag{14}$$

We see that in order to maximize the amplitude gain, the population is not completely inverted (that would be $\rho_{11} = 1$, $\rho_{00} = 0$). For a complete population inversion to happen, the following condition has to be fulfilled:

$$\frac{\rho_{11}}{\rho_{00}} \gg 1 \quad \Rightarrow \quad \frac{\Gamma_{21}}{\Gamma_{10}} \gg \frac{2\Gamma_{21}\gamma_{20}}{\Omega_d^2}. \tag{15}$$

This could be achieved by further increasing the drive strength Ω_d. However, if we look at the expression for the reflection in equation (6), we see that increasing the pumping strength towards infinity would make the reflection revert to 1. This trade-off explains why we do not achieve a maximum amplitude gain of $\sqrt{2}$ (a power gain of 2), which would be the result if an incoming photon would stimulate emission of another photon from a perfectly inverted atom.

2.4. Correction with pure dephasing

Now we discuss the effect of pure dephasing on the previous results. Neglecting terms of order $\mathcal{O}(\Gamma_{10}/\Gamma_{21})$, the reflection coefficient on resonance with pure dephasing included can be written as

$$r = 1 + 2\frac{\Gamma_{10}}{\gamma_{10}}\frac{(\eta - 1)}{(\eta + 1)\left(\eta\frac{\Gamma_{10}\gamma_{20}}{\gamma_{21}\gamma_{10}} + 2\right)} \tag{16}$$

with $\eta = \frac{\Omega_d^2}{2\Gamma_{10}\gamma_{20}}$. Maximizing this expression, we find the optimal value for η:

$$\eta_{\max} = 1 + \eta_c, \quad \eta_c = \sqrt{2\left(1 + 2\frac{\gamma_{21}\gamma_{10}}{\Gamma_{10}\gamma_{20}}\right)}. \tag{17}$$

Hence, the optimal drive strength including pure dephasing is

$$\Omega_d^2 = 2\Gamma_{10}\gamma_{20}\,(1 + \eta_c)\,, \tag{18}$$

for which we obtain the maximum reflection

$$r = 1 + 2\frac{\Gamma_{10}}{\gamma_{10}}\frac{1}{\left[1 + \sqrt{2}\left(1 + 2\frac{\gamma_{21}\gamma_{10}}{\Gamma_{10}\gamma_{20}}\right)^{-1/2}\right]\left[\left(\sqrt{2\left(1 + 2\frac{\gamma_{21}\gamma_{10}}{\Gamma_{10}\gamma_{20}}\right)} + 1\right)\frac{\Gamma_{10}\gamma_{20}}{\gamma_{21}\gamma_{10}} + 2\right]}. \tag{19}$$

2.5. Experimental feasibility

We now apply the theoretical results above to a typical experimental system of a superconducting transmon qubit [92] to see what the optimal parameters for an experiment would be, and whether they are within reach for currently available devices. By shorting one end of the transmission line to create an effective mirror, the decay rates Γ_{10} and Γ_{21} become a function of the transition frequency ω_{10} of the energy levels [52]

$$\Gamma_{10} = 2\Gamma_{10}^{\mathrm{TL}}\cos^2\left[\frac{L}{v}\omega_{10}\right], \tag{20}$$

$$\Gamma_{21} = 2\Gamma_{21}^{\mathrm{TL}}\cos^2\left[\frac{L}{v}(\omega_{10} + \alpha)\right], \tag{21}$$

where $\Gamma_{10}^{\mathrm{TL}}/2\pi = 37.5$ MHz and $\Gamma_{21}^{\mathrm{TL}}/2\pi \approx 2\Gamma_{10}^{\mathrm{TL}}/2\pi = 75$ MHz are the bare relaxation rates in an open transmission line, $\alpha = \omega_{21} - \omega_{10} = -2\pi \times 440$ MHz is the anharmonicity between the transition frequencies, $L = 33$ mm is the distance between the transmon and the mirror, and $v = 9 \times 10^7$ m s^{-1} is the speed of light in the transmission line. The given values are typical for this kind of setup [33, 52].

The transition frequencies of the transmon are tunable *in situ* by an external magnetic flux, so we want to find the resonance frequency ω_{10} that gives the highest possible reflection. We therefore express the

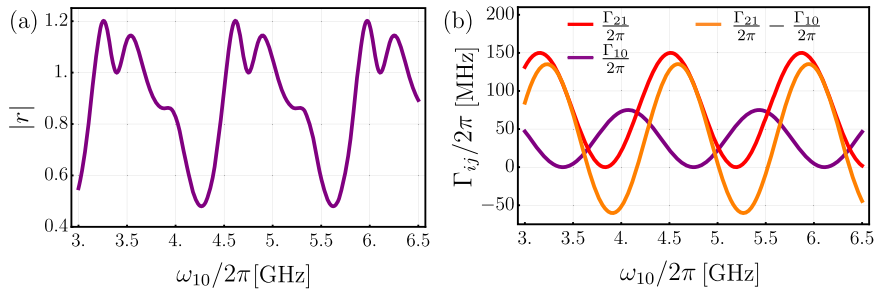

Figure 3. Reflection coefficient and decay rates as functions of transition frequency. (a) Absolute value of the reflection coefficient as a function of transition frequency ω_{10} at drive strength $\Omega_d/2\pi = 59.5$ MHz and pure dephasing $\Gamma_{10}^{\phi}/2\pi = 1.65$ MHz, $\Gamma_{21}^{\phi}/2\pi = \Gamma_{20}^{\phi}/2\pi = 5$ MHz. (b) The decay rates $\Gamma_{10}/2\pi$ (purple) and $\Gamma_{21}/2\pi$ (red), and their difference $\Gamma_{21}/2\pi - \Gamma_{10}/2\pi$ (orange), as a function of the transition frequency ω_{10}.

reflection as a function of the drive strength Ω_d and the frequency ω_{10}, using equations (20) and (21), and maximize this function numerically. A plot of the resulting reflection amplitude can be seen in figure 3(a). With the above parameters and pure dephasing rates of $\Gamma_{10}^{\phi}/2\pi = 1.65$ MHz, $\Gamma_{21}^{\phi}/2\pi = \Gamma_{20}^{\phi} = 5$ MHz, again chosen from typical values [33, 49, 52] and optimal drive strength $\Omega_d/2\pi = 59.5$ MHz, the reflection reaches a maximum of 1.2 which corresponds to an amplitude gain of 20%. Due to the non-zero dephasing, this is lower than the theoretical limit of 25% calculated above. We note that dephasing and non-radiative decay rates can be lower than what we have assumed here, as shown, e.g., in references [47, 57].

We find that there are two local maxima for the gain in figure 3(a), located in the area close to the nodes of the decay rate Γ_{10} [see figure 3(b)], e.g., between $\omega_{10}/2\pi \approx 4.5$ GHz and $\omega_{10}/2\pi \approx 5.0$ GHz. This is the area where the requirement for amplification $\Omega_d^2 > 3\Gamma_{10}\Gamma_{21}$ is fulfilled. Between the two local maxima, we find a local minimum with a 0% gain. This local minimum occurs at the node of the electromagnetic field, where the decay rate Γ_{10} goes to zero and no transition from $|1\rangle$ to $|0\rangle$ is possible [see figure 3(b)].

We note that if tuning the qubit frequency to the maxima in figure 3(a) is required, the amplifier will be limited to working at these frequencies, with rather narrow bandwidth. However, this bandwidth can be increased by making the mirror itself tunable, e.g., by placing a superconducting quantum interference device at the end of the waveguide [50, 51, 93]. In this way, the interference can be changed such that the maxima are moved to other qubit frequencies.

We also note that driving the $|0\rangle \leftrightarrow |2\rangle$ transition directly is hard in a transmon due to selection rules [92]. It is possible to drive the transition with a two-photon drive instead, where the frequencies of two drive photons sum up to ω_{20}. However, if this drive is too strong, the qubit states will be dressed and we will instead have a setup like that discussed in section 4. Another solution is to use another superconducting qubit which does not suffer from this limitation on allowed transitions, e.g., the flux qubit, as was done in reference [36].

Finally, if the $|0\rangle \leftrightarrow |2\rangle$ transition is driven through the waveguide, the strength with which the drive couples to the system will be frequency-dependent in the same way as in equation (20), with ω_{10} replaced by ω_{20}. As long as the drive frequency does not correspond to a node of the field at the atom, a decrease or increase in coupling strength can be compensated by adjusting the input drive power. It would also be possible to avoid any such issues by driving the atom through a separate line not affected by the interference with the mirror.

3. Amplification with a strongly driven two-level atom in front of a mirror

The next setup we consider is a two-level atom in front of a mirror that is driven strongly on resonance, as depicted in figure 1(c). The strong driving results in a splitting of the atomic energy levels such that the dynamics are best understood in terms of dressed states. As shown theoretically in references [77, 78] and experimentally in references [33–35], amplification can be achieved in this setup through higher-order processes when probing at frequencies in-between those of the Mollow triplet.

3.1. Hamiltonian and equations of motion

The Hamiltonian of a driven two-level system, with ground state $|0\rangle$ and excited state $|1\rangle$, interacting with the continuum of modes in the semi-infinite waveguide, is, in a frame rotating with the drive frequency ω_d,

$$H = H_{\rm a} + H_{\rm f} + H_{\rm int}, \tag{22}$$

$$H_{\rm a} = \delta\omega_{10}\sigma_{11} + E\left(\sigma_{\rm t} + \sigma_{\rm t}^{\dagger}\right), \tag{23}$$

$$H_{\rm f} = \int {\rm d}\omega\ \omega a^{\dagger}(\omega)a(\omega), \tag{24}$$

$$H_{\rm int} = \frac{1}{\sqrt{2\pi}}\int_0^{\infty} {\rm d}\omega\left(a^{\dagger}(\omega)\sigma_{\rm t} + \sigma_{\rm t}^{\dagger}a(\omega)\right), \tag{25}$$

where $\delta\omega_{10} = \omega_{10} - \omega_{\rm d}$, $\Omega_{\rm d} = 2\sqrt{\Gamma_{10}}E$, $|E|^2$ is the number of incoming drive photons per second, $\sigma_{\rm t} = \sqrt{\Gamma_{10}}\sigma_{01}$, and $a^{\dagger}(\omega)$ $[a(\omega)]$ are the photon creation [annihilation] operators at frequency ω. We calculate the eigenenergies ω_g, ω_e and the corresponding dressed eigenstates $|g\rangle$, $|e\rangle$ of the atomic Hamiltonian $H_{\rm a}$ in equation (23), and define the population and transition operators for the dressed states as

$$\sigma_{\mu\nu} = |\mu\rangle\langle\nu|, \tag{26}$$

where $\mu, \nu \in \{g, e\}$. The equation of motion of the dressed state operators $\sigma_{\mu\nu}$ is given by the Heisenberg equations of motion. The solution is divided into a steady state and linear-response part, $\langle\sigma_{\mu\nu}\rangle = \langle\sigma_{\mu\nu}\rangle_{\rm S} + \langle\sigma_{\mu\nu}\rangle_{\rm L} e^{{\rm i}(\omega_{\rm d}-\omega_{\rm p})t}$. The derivation and solution of the equations of motion, which closely follows that for a three-level atom in an open waveguide in reference [40], is given in appendix B. The main difference is that, in an open waveguide, the atom couples to two continua of modes in the waveguide, one right-moving and one left-moving, which both enter in equation (25). This means that $\sigma_{\rm t} = \sqrt{\Gamma_{10}/2}\sigma_{01}$ in the open-waveguide case receives an additional factor of two for the case with the mirror $\sigma_{\rm t} = \sqrt{\Gamma_{10}}\sigma_{01}$. In the end, these differences lead to a twice as large gain in the amplification for the mirror as we will see in the following.

3.2. Amplification

The reflection coefficient is defined by the ratio of the outgoing field $\langle a_{\rm out}\rangle$ and the incoming field $\langle a_{\rm in}\rangle$

$$r = \frac{\langle a_{\rm out}\rangle}{\langle a_{\rm in}\rangle}, \tag{27}$$

For the two-level system with $\delta\omega_{10} = 0$, the reflection coefficient becomes

$$r = 1 - \frac{2\Gamma_{10}^2\left(\Gamma_{10}^3 - 3i\Gamma_{10}^2\delta - 2\Gamma_{10}\delta^2 + 2i\delta\Omega_{\rm d}^2\right)}{(\Gamma_{10} - 2i\delta)\left(\Gamma_{10}^2 + 2\Omega_{\rm d}^2\right)\left(\Gamma_{10}^2 - 3i\Gamma_{10}\delta - 2\delta^2 + 2\Omega_{\rm d}^2\right)}, \tag{28}$$

where $\delta = \omega_{10} - \omega_{\rm p}$. More details of the calculation are given in appendix B.

By maximizing $|r|$ using equation (28), we find that the maximum possible amplitude gain is $|r| \approx 1.069$; it is achieved for the drive amplitude $\Omega_{10} \approx 2\Gamma_{10}$ and probe detuning of $\delta \approx \pm 1.2\Gamma_{10}$. It is interesting to note that the experiment in reference [33] appears to have come very close to this theoretical maximum. We also note that the numerical simulation in reference [33] coincides with our analytical result.

Performing a similar analysis of the reflection coefficient for a two-level system in an open waveguide, we find that the maximum reflection for the same drive amplitude and detuning is only given by $|r|^2 \approx 1.034$, which is only half of the gain for the atom in front of a mirror. This makes sense, since the atomic output is divided between two propagation directions in the open waveguide, while it is collected in a single output channel when a mirror is included.

In figure 4(a), we plot the reflection coefficient of the strongly driven two-level system as a function of the detuning δ of the probe frequency and the drive strength $\Omega_{\rm d}$ for resonant drive. The bright areas correspond to gain and the dark areas to attenuation. We can see how gain is achieved at probe frequencies in-between the frequencies corresponding to the Mollow triplet. In figure 4(b), the linecut of figure 4(a) is depicted. The blue curve, showing the reflection of the two-level system in front of a mirror, has a higher maximum gain than the reflection of the two-level system in an open waveguide, seen as a comparison by the purple dashed curve. This coincides with the analysis of the reflection coefficient above.

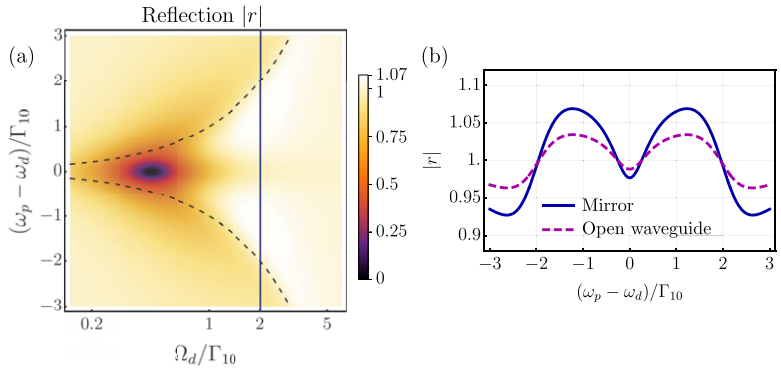

Figure 4. Maximizing the reflection coefficient of a strongly driven two-level system in front of a mirror. (a) Reflection coefficient $|r|$ of a weak probe for resonant drive ($\omega_d - \omega_{10} = 0$) as a function of the detuning of the probe frequency and drive amplitude. The maximum possible amplitude gain can be seen in the bright areas around $\Omega_d \approx 2\Gamma_{10}$ (marked by the solid line) and $(\omega_p - \omega_{10}) \approx \pm 1.2\Gamma_{10}$. The optimal drive strength is the same for both the mirror and open-waveguide case. (b) A plot of the linecut at $\Omega_d = 2\Gamma_{10}$ in (a). It compares the reflection of a two-level system in front of a mirror (blue, the linecut) to that in an open waveguide (purple, dashed). In both cases, we observe a maximum gain around $(\omega_p - \omega_{10}) \approx \pm 1.2\Gamma_{10}$, but the gain for the atom in front of a mirror is around 6.9%, around twice the gain for the atom in an open waveguide, which is around 3.4%.

4. Amplification with a strongly two-photon-driven three-level atom in front of a mirror

For our last setup, we consider a strongly driven three-level atom in front of a mirror, with the drive at half the $|0\rangle \leftrightarrow |2\rangle$ transition frequency, as sketched in figure 1(d). As shown experimentally for an open waveguide in reference [40], amplification can be achieved in this setup through population inversion among the dressed states of the three-level atom.

4.1. Hamiltonian and equations of motion

We consider the same Hamiltonian as for the two-level case, equations (22)–(25), but including the third atomic level in the bare atomic Hamiltonian and in the Hamiltonian describing the interaction between the atom and the waveguide. The atom Hamiltonian in equation (23) is modified to read,

$$H_a = \delta_{10}\sigma_{11} + \delta_{20}\sigma_{22} + E\left(\sigma_t + \sigma_t^\dagger\right), \tag{29}$$

where $\delta_{10} = \omega_{10} - \omega_d$, $\delta_{20} = \omega_{20} - 2\omega_d$, and $\sigma_t = \sqrt{\Gamma_{10}}\sigma_{01} + \sqrt{\Gamma_{21}}\sigma_{12}$. This new expression for σ_t is the only change required in the interaction Hamiltonian in equation (25).

We set up and solve the equations of motion for the dressed-state operators $\sigma_{\mu\nu}$ in the same way as for the two-level system in section 3.1, but with $\mu, \nu \in \{g, m, e\}$, where $\{g, m, e\}$ are the dressed states of the three-level system. As shown in detail in appendix B, the equations for the steady-state and linear-response components of the reflected probe signal are the same as for the two-level system in section 3.1, except for the new definitions of variables given here.

4.2. Amplification

In figure 5, we plot the numerically computed reflection coefficient for a weak probe as a function of probe frequency ω_p and drive amplitude $\Omega_d = 2E\sqrt{\Gamma_{10}}$ for typical experimental parameters [40]. We observe a maximum amplitude gain of ~6%. The largest gains are observed when the probe is close to resonant with one of the dressed-state transitions $|m, N\rangle \leftrightarrow |e, N+1\rangle$ and $|g, N\rangle \leftrightarrow |m, N+1\rangle$.

Since the population inversion among dressed states is essential for the amplification in this system, we explore further whether we can increase this population inversion by tuning the ratio between relaxation rates for the different atomic transitions. We consider the reflection along the branches for resonant probing, which are shown by the dashed black lines in figure 5. The expression for the reflection on resonance $\omega_p = \omega_d + \omega_\nu - \omega_\mu$ can be simplified to [40]

$$r = 1 + \frac{|\langle\mu|\,\sigma_t\,|\nu\rangle|^2}{\xi_{\mu\nu\mu'\nu'}}\left(\langle\sigma_{\nu\nu}\rangle_S - \langle\sigma_{\mu\mu}\rangle_S\right). \tag{30}$$

This equation shows that population inversion among the dressed states leads to a gain in the reflection, whereas we obtain attenuation for non-inverted population.

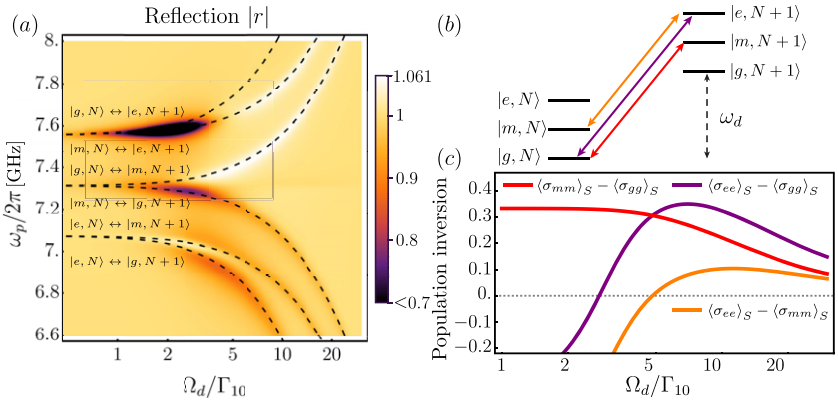

Figure 5. Amplification through population inversion among the dressed states of a strongly driven three-level atom. (a) Reflection as a function of the probe frequency ω_p and drive amplitude Ω_d for a drive frequency of $\omega_\mathrm{d}/2\pi = 7.26$ GHz for a three-level system in front of a mirror with the transition frequencies $\omega_{10}/2\pi = 7.4$ GHz, $\omega_{20} = 2\omega_\mathrm{d}$, and the relaxation rates $\Gamma_{10}/2\pi = 40$ MHz, $\Gamma_{21} = 2\Gamma_{10}$. The dashed lines show the possible transitions between dressed states in the system. The dark region at $\omega_\mathrm{p}/2\pi \approx 7.58$ GHz is outside of the plot range, since the reflection is low. (b) Sketch of the dressed states. The arrows demonstrating the transitions correspond to the three upper branches in panel (a). (c) Matrix elements of the steady-state solution showing the (non-)inverted population. Population inversion occurs for positive values of $\langle\sigma_{\mu\mu}\rangle_\mathrm{S} - \langle\sigma_{\nu\nu}\rangle_\mathrm{S}$, $\mu > \nu$, which is indicated by the grey dashed line at 0. The colors of the curves correspond to the colors of the arrows in (b).

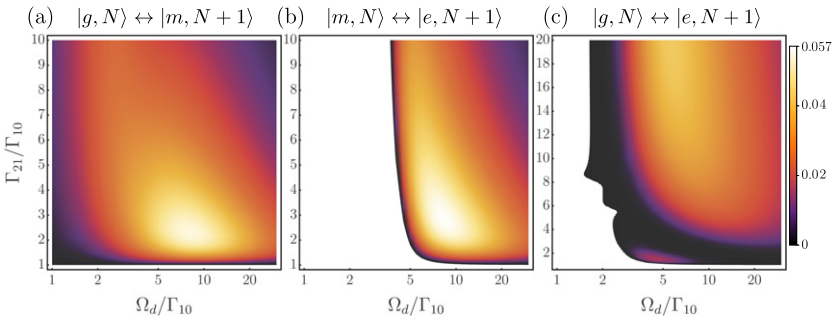

Figure 6. Gain of a resonant probe for the upper branches of figure 5 as a function of the drive amplitude $\Omega_\mathrm{d}/\Gamma_{10}$ and the ratio Γ_{21}/Γ_{10} between the decay rates. (a) Resonant gain on the $|g,N\rangle \leftrightarrow |m,N+1\rangle$ transition. We find a maximum gain of around 5.5% for $\Omega_\mathrm{d}/\Gamma_{10} = 8$ and $\gamma_{21}/\gamma_{10} = 2.3$. (b) Resonant gain on the $|m,N\rangle \leftrightarrow |e,N+1\rangle$ transition. We find a maximum gain of around 5.7% for $\Omega_\mathrm{d}/\Gamma_{10} = 8.5$ and $\Gamma_{21}/\Gamma_{10} = 2.8$. The white area in the left part of the plot corresponds to non-inverted population, i.e., 'negative gain' (attenuation). This area corresponds to the dark spot at $\omega_\mathrm{p}/2\pi \approx 7.6$ GHz in figure 5. (c) Resonant gain on the $|g,N\rangle \leftrightarrow |e,N+1\rangle$ transition. Here, the gain increases around $\Omega_\mathrm{d}/\Gamma_{10} = 5$ for increasing Γ_{21}/Γ_{10}. However, the maximum gain even for $\Gamma_{21}/\Gamma_{10} = 20$ is still smaller than the maximum gains on the other transitions.

In figure 6, we plot the second term of the right-hand side in equation (30), which corresponds to the gain, for the upper branches in figure 5, as a function of the drive strength Ω_d and the ratio of the decay rates Γ_{21}/Γ_{10}. The bright parts of the panels in figure 6 correspond to the highest resonant gains. Selecting the values for the drive strength $\Omega_\mathrm{d}/\Gamma_{10}$ and the ratio of the decay rates Γ_{21}/Γ_{10} that give the highest resonant gain, we find a maximum gain of 6.2% by searching around the resonance frequency of the $|g,N\rangle \leftrightarrow |m,N+1\rangle$ [figure 6(a)] transition for $\Omega_\mathrm{d}/\Gamma_{10} = 8$ and $\Gamma_{21}/\Gamma_{10} = 2.3$. The corresponding gain for a transmon qubit in an open transmission line is around 3%. Note that for a transmon in an open transmission line, Γ_{21}/Γ_{10} is always 2 (assuming a flat spectral density for the transmission line). The mirror allows us to tune Γ_{21}/Γ_{10} to achieve a higher gain, but the increase is small, since the optimal ratio of relaxation rates is close to 2. Thus, the main contribution of the mirror to the increased gain is to direct all atomic output in one direction.

Repeating the same optimization for the $|m,N\rangle \leftrightarrow |e,N+1\rangle$ transition in figure 6(b), we find a maximum gain of 6.1% for $\Omega_\mathrm{d}/\Gamma_{10} = 8.5$ and $\Gamma_{21}/\Gamma_{10} = 2.8$. Once again, the optimal ratio of relaxation rates is close to 2, meaning that the improvement in gain compared to the open-transmission-line case is just a little more than a factor 2. The $|g,N\rangle \leftrightarrow |e,N+1\rangle$ transition [figure 6(c)] differs from the previous two in that the highest amplification is found when $\Gamma_{21} \gg \Gamma_{10}$. However, the maximum gain around this transition is smaller than that close to the other two transitions.

Table 1. A summary of the results in the article. We compare the highest amplitude gain we found for each of the three setups with a mirror in figure 1 to the highest amplitude gain found or observed for the same systems in an open waveguide.

Setup	3 levels, $\omega_d = \omega_{20}$	2 levels, $\omega_d = \omega_{10}$	3 levels, $\omega_d = \omega_{20}/2$
Schematic	1(b)	1(c)	1(d)
Gain with mirror	25%	6.9%	6.2%
Gain in open waveguide	12.5%	3.4%	3%

5. Discussion and conclusion

In this article, we have investigated three different types of single-atom amplifiers, using population inversion, higher-order multi-photon processes, and hidden inversion in the dressed-state basis. For all these schemes, we compared the maximum achievable amplitude gain with the atom placed in front of a mirror versus when the atom was coupled to an open waveguide. The results are summarized in table 1. We note that first setup with a mirror reached an amplitude gain not too far from the absolute theoretical limit of $\sqrt{2}$, which corresponds to perfect population inversion and perfect stimulated emission.

We found that for all schemes, the gain is enhanced by the mirror, mainly because of two reasons:

(a) The mirror reduces the number of output channels for the electromagnetic field from two in an open waveguide to one. All output from the atom is thus contributing to the gain instead of only half.

(b) The mirror creates standing waves of the electromagnetic field through interference such that the strength of the coupling between the atom and the field becomes sensitive to the atomic position and transition frequencies. This makes it possible to tune the ratio of decay rates for different atomic transitions to increase population inversion and thus enhance amplification.

These insights are ready to be demonstrated in experiments with superconducting qubits in waveguide QED, but could also find applications in other platforms for waveguide QED. Specifically, we showed that our set-ups can be implemented with a transmon coupled to a 1D semi-infinite transmission line with currently available technology (at least two such experiments [33, 40] have already come close to the limits in table 1). We believe that this can prove useful for on-chip amplification to improve signal-to-noise ratios in experiments in quantum information and quantum optics.

An important direction for future work is to investigate how the achievable gain changes if more qubits are added to the setups described here. For example, one could imagine a cascaded setup of atoms in front of mirrors with circulators ensuring unidirectional propagation from one mirror to the next, as shown to enhance photon detection with three-level atoms in reference [94]. It could also be interesting to check how the anharmonicity of the qubit affects the gain for the three-level system with a two-photon drive.

Acknowledgements

EW acknowledges funding from the Swedish Research Council (VR) through Grant No. 2016-06059. ICH acknowledges financial support from the MOST of Taiwan under project 109-2636-M-007-007 and the Center for Quantum Technology from the Featured Areas Research Center Program within the framework of the Higher Education Sprout Project by the Ministry of Education (MOE) in Taiwan. AFK and PD acknowledge support from the Knut and Alice Wallenberg Foundation through the Wallenberg Centre for Quantum Technology (WACQT). AFK acknowledges support from the Swedish Research Council (Grant Number 2019-03696).

Data availability statement

No new data were created or analysed in this study.

Appendix A. Details of the derivation of the reflection coefficient for a strongly driven three-level atom in front of a mirror

In this appendix, we provide the details of the derivation of the results presented in section 2. Starting from the setup described by the equations in section 2.1, we assume that the probe on the $|0\rangle \leftrightarrow |1\rangle$ is weak, i.e.,

$\Omega_{10}/\Gamma_{10} \ll 1$. Solving the master equation for the steady state ($\dot{\rho} = 0$), we obtain [36]

$$\rho_{00} = \frac{A}{A+B+1}, \qquad \rho_{11} = \frac{B}{A+B+1}, \qquad \rho_{22} = \frac{1}{A+B+1}, \tag{A.1}$$

$$\rho_{10} = \frac{i\frac{\Omega_p}{2\lambda_{10}}\left(\frac{\Omega_d^2}{4\lambda_{02}\lambda_{12}}(\rho_{00}-\rho_{22})+\rho_{11}-\rho_{00}\right)}{1+\frac{\Omega_d^2}{4\lambda_{10}\lambda_{12}}}, \tag{A.2}$$

where

$$A = \frac{\rho_{00}}{\rho_{22}} = \frac{2\Gamma_{21}|\lambda_{02}|^2}{\gamma_{20}\Omega_d^2} + 1, \qquad B = \frac{\rho_{11}}{\rho_{22}} = \frac{\Gamma_{21}}{\Gamma_{10}}, \tag{A.3}$$

and $\lambda_{ij} = \lambda_{ji}^*$ with

$$\lambda_{10} = \gamma_{10} + i\delta\omega_{10}, \qquad \lambda_{12} = \gamma_{21} - i\delta\omega_{20} + i\delta\omega_{10}, \qquad \lambda_{02} = \gamma_{20} - i\delta\omega_{20}. \tag{A.4}$$

We now assume that $\Gamma_{21} \gg \Gamma_{10}$ to ensure population inversion. From equations (A.1) and (A.3), we see that the second excited state then is nearly unpopulated. Neglecting terms of order $\mathcal{O}(\Gamma_{10}/\Gamma_{21})$, this gives

$$\rho_{10} \approx i\frac{\Omega_p(\rho_{11}-\rho_{00})}{2\lambda_{10}+\frac{\Omega_d^2}{2\lambda_{12}}}. \tag{A.5}$$

The reflection coefficient is given by [52, 56]

$$r = 1 - 2i\frac{\Gamma_{10}}{\Omega_p}\langle\sigma_{01}\rangle = 1 - 2i\frac{\Gamma_{10}}{\Omega_p}\rho_{10} = 1 + 2\Gamma_{10}\frac{(\rho_{11}-\rho_{00})}{2\lambda_{10}+\frac{\Omega_d^2}{2\lambda_{12}}}. \tag{A.6}$$

As mentioned in the main text, this is where our derivation deviates from that in reference [36] for an open waveguide. The mirror adds a factor 2 to the second term of the reflection coefficient compared to the open waveguide.

From equation (A.6), it is clear that amplification requires $\rho_{11} > \rho_{00}$, which leads to

$$\frac{\Gamma_{21}}{\Gamma_{10}} > \frac{2\Gamma_{21}|\lambda_{02}|^2}{\gamma_{20}\Omega_d^2} + 1 \Rightarrow \Omega_d^2 > \frac{2\Gamma_{10}|\lambda_{02}|^2}{\gamma_{20}} + \frac{\Omega_d^2\Gamma_{10}}{\Gamma_{21}} \approx \frac{2\Gamma_{10}|\lambda_{02}|^2}{\gamma_{20}}. \tag{A.7}$$

For a resonant drive, $\delta\omega_{20} = 0$, this reduces to

$$\Omega_d^2 > 2\Gamma_{10}\gamma_{20}. \tag{A.8}$$

If we further assume no pure dephasing, we have $\gamma_{20} = \Gamma_{21}/2$ and thus

$$\Omega_d^2 > \Gamma_{10}\Gamma_{21}. \tag{A.9}$$

We now calculate the maximal possible amplitude gain of the single-atom amplifier. We consider double resonance, $\delta\omega_{20} = \delta\omega_{10} = 0$, and no pure dephasing, i.e., $\gamma_{10} = \Gamma_{10}/2$, $\gamma_{21} = \Gamma_{21}/2$, and $\gamma_{20} = \Gamma_{21}/2$. We can then rewrite the populations in equation (7) as $\rho_{00} = 1/(1+\nu)$ and $\rho_{11} = \nu/(1+\nu)$ with $\nu = \Omega_d^2/(\Gamma_{10}\Gamma_{21})$, which leads to the reflection coefficient

$$r = 1 + 2\frac{(\nu-1)}{(1+\nu)^2}. \tag{A.10}$$

This expression reaches its maximum value for $\nu = 3$, which is achieved when

$$\Omega_d^2 = 3\Gamma_{10}\Gamma_{21}, \tag{A.11}$$

which is equation (11) in the main text.

Appendix B. Equations of motion for a strongly driven atom in front of a mirror

In this appendix, we derive the equations of motion for the strongly driven atom in front of a mirror. The derivation applies both for the two-level atom in section 3 and the three-level atom in section 4. We start with the diagonalised form of the two-level Hamiltonian H_a^2 and three-level Hamiltonian H_a^3, given by

$$H_{\mathrm{a}}^{2} = \omega_g \sigma_{gg} + \omega_e \sigma_{ee}, \tag{B.1}$$

$$H_{\mathrm{a}}^{3} = \omega_g \sigma_{gg} + \omega_m \sigma_{mm} + \omega_e \sigma_{ee}. \tag{B.2}$$

The field and interaction Hamiltonians are

$$H_{\mathrm{f}} = \int \mathrm{d}\omega\ \omega a^{\dagger}(\omega) a(\omega), \tag{B.3}$$

$$H_{\mathrm{a-f}} = \frac{1}{\sqrt{2\pi}} \int_0^{\infty} \mathrm{d}\omega \left(a^{\dagger}(\omega)\sigma_{\mathrm{t}} + \sigma_{\mathrm{t}}^{\dagger} a(\omega) \right), \tag{B.4}$$

with $\sigma_{\mathrm{t}} = \sqrt{\Gamma_{10}}\sigma_{01}$ for the two-level system, and $\sigma_{\mathrm{t}} = \sqrt{\Gamma_{10}}\sigma_{01} + \sqrt{\Gamma_{21}}\sigma_{12}$ for the three-level system.

In the following, we denote the dressed-state operators by $\sigma_{\mu\nu}$ and the dressed-state transition frequencies by $\omega_{\mu\nu} = \omega_{\mu} - \omega_{\nu}$, with $\mu, \nu \in \{g, m, e\}$ for the three-level atom and $\mu, \nu \in \{g, e\}$ for the two-level atom. The equation of motion for $\sigma_{\mu\nu}$ can be calculated by the Heisenberg equation

$$\frac{\mathrm{d}}{\mathrm{d}t}\sigma_{\mu\nu} = i\left[H, \sigma_{\mu\nu}\right]. \tag{B.5}$$

The commutator for the atom part of the three-level system is given by

$$\begin{aligned} i\left[H_{\mathrm{a}}^{3}, \sigma_{\mu\nu}\right] &= i\left[\omega_g \sigma_{gg} + \omega_m \sigma_{mm} + \omega_e \sigma_{ee}, \sigma_{\mu\nu}\right] \\ &= \omega_g \left(|g\rangle \overbrace{\langle g|\mu\rangle}^{\delta_{g\mu}} \langle \nu| - |\mu\rangle \overbrace{\langle \nu|g\rangle}^{\delta_{\nu g}} \langle g| \right) \\ &\quad + \omega_m \left(|m\rangle \overbrace{\langle m|\mu\rangle}^{\delta_{m\mu}} \langle \nu| - |\mu\rangle \overbrace{\langle \nu|m\rangle}^{\delta_{\nu m}} \langle m| \right) \\ &\quad + \omega_e \left(|e\rangle \overbrace{\langle e|\mu\rangle}^{\delta_{e\mu}} \langle \nu| - |\mu\rangle \overbrace{\langle \nu|e\rangle}^{\delta_{\nu e}} \langle e| \right) \\ &= i\left(\omega_{\mu} - \omega_{\nu}\right)\sigma_{\mu\nu}. \end{aligned} \tag{B.6}$$

The result for the two-level system is the same, but the calculation does not contain terms with $\omega_m \sigma_{mm}$. For the interaction part we find

$$\begin{aligned} i\left[H_{\mathrm{a-f}}, \sigma_{\mu\nu}\right] &= \frac{i}{\sqrt{2\pi}} \int_0^{\infty} \mathrm{d}\omega \left(a^{\dagger}(\omega)\left[\sigma_{\mathrm{t}}, \sigma_{\mu\nu}\right] + \left[\sigma_{\mathrm{t}}^{\dagger}, \sigma_{\mu\nu}\right] a(\omega) \right) \\ &= \frac{i}{\sqrt{2\pi}} \int_0^{\infty} \mathrm{d}\omega a^{\dagger}(\omega)\left[\sigma_{\mathrm{t}}, \sigma_{\mu\nu}\right] + \frac{i}{\sqrt{2\pi}} \int_0^{\infty} \mathrm{d}\omega \left[\sigma_{\mathrm{t}}^{\dagger}, \sigma_{\mu\nu}\right] a(\omega). \end{aligned} \tag{B.7}$$

In the same way, we calculate the equation of motion for $a(\omega)$:

$$\begin{aligned} \dot{a}(\omega) &= i\int_{-\infty}^{\infty} \mathrm{d}\omega\omega' \left[a^{\dagger}(\omega)a(\omega), a(\omega')\right] + i\int_{-\infty}^{\infty} \mathrm{d}\omega \sqrt{\frac{1}{2\pi}} \left[a^{\dagger}(\omega)\sigma_{\mathrm{t}}, a(\omega')\right] \\ &= -i\omega a(\omega) - \frac{i}{\sqrt{2\pi}}\sigma_{\mathrm{t}}. \end{aligned} \tag{B.8}$$

The solution of equation (B.8) can be written as

$$a(\omega) = \mathrm{e}^{-\mathrm{i}\omega(t-t_0)} a_0(\omega) - \frac{i}{\sqrt{2\pi}} \int_{t_0}^{\mathrm{t}} \mathrm{d}t' \sigma_{\mathrm{t}}\left(t'\right) \mathrm{e}^{-\mathrm{i}\omega\left(t-t'\right)}. \tag{B.9}$$

Inserting this solution into equation (B.7), we find

$$\begin{aligned} \frac{i}{\sqrt{2\pi}} \int_0^{\infty} \mathrm{d}\omega a^{\dagger}(\omega)\left[\sigma_{\mathrm{t}}, \sigma_{\mu\nu}\right] &= \frac{i}{\sqrt{2\pi}} \int_0^{\infty} \mathrm{d}\omega \mathrm{e}^{\mathrm{i}\omega(t-t_0)} a_0^{\dagger}(\omega)\left[\sigma_{\mathrm{t}}, \sigma_{\mu\nu}\right] \\ &\quad - \frac{1}{2\pi} \int_{t_0}^{\mathrm{t}} \mathrm{d}t' \int_0^{\infty} \mathrm{d}\omega \mathrm{e}^{\mathrm{i}\omega\left(t-t'\right)} \sigma_{\mathrm{t}}^{\dagger}\left(t'\right)\left[\sigma_{\mathrm{t}}, \sigma_{\mu\nu}\right] \end{aligned}$$

$$= -ia_{\text{in}}^{\dagger}\left[\sigma_{\text{t}},\sigma_{\mu\nu}\right]-\int_{t_0}^{\text{t}}\text{d}t'\,\delta\left(t-t'\right)\sigma_{\text{t}}^{\dagger}\left(t'\right)\left[\sigma_{\text{t}},\sigma_{\mu\nu}\right]$$

$$= -ia_{\text{in}}^{\dagger}\left[\sigma_{\text{t}},\sigma_{\mu\nu}\right]-\frac{1}{2}\sigma_{\text{t}}^{\dagger}\left[\sigma_{\text{t}},\sigma_{\mu\nu}\right], \tag{B.10}$$

and

$$\begin{aligned}\frac{i}{\sqrt{2\pi}}\int_0^{\infty}\text{d}\omega a(\omega)\left[\sigma_{\text{t}}^{\dagger},\sigma_{\mu\nu}\right] &= \frac{i}{\sqrt{2\pi}}\int_0^{\infty}\text{d}\omega\text{e}^{-\text{i}\omega(t-t_0)}a_0(\omega)\left[\sigma_{\text{t}}^{\dagger},\sigma_{\mu\nu}\right]\\ &\quad+\frac{1}{2\pi}\int_{t_0}^{\text{t}}\text{d}t'\int_0^{\infty}\text{d}\omega\text{e}^{-\text{i}\omega\left(t-t'\right)}\left[\sigma_{\text{t}}^{\dagger},\sigma_{\mu\nu}\right]\sigma_{\text{t}}\left(t'\right)\\ &= i\left[\sigma_{\text{t}}^{\dagger},\sigma_{\mu\nu}\right]a_{\text{in}}+\int_{t_0}^{\text{t}}\text{d}t'\delta\left(t'-t\right)\left[\sigma_{\text{t}}^{\dagger},\sigma_{\mu\nu}\right]\sigma_{\text{t}}\left(t'\right)\\ &= i\left[\sigma_{\text{t}}^{\dagger},\sigma_{\mu\nu}\right]a_{\text{in}}+\frac{1}{2}\left[\sigma_{\text{t}}^{\dagger},\sigma_{\mu\nu}\right]\sigma_{\text{t}},\end{aligned} \tag{B.11}$$

where we used

$$\int_{t_0}^{\text{t}}\text{d}t'\sigma_{\text{t}}\left(t'\right)\delta\left(t-t'\right)=\frac{1}{2}\sigma_{\text{t}}(t) \tag{B.12}$$

and defined

$$a_{\text{in}}(t)=\frac{1}{\sqrt{2\pi}}\int_{-\infty}^{\infty}\text{d}\omega\text{e}^{-\text{i}\omega(t-t_0)}a_0(\omega). \tag{B.13}$$

Combining the above results, the equation of motion for $\sigma_{\mu\nu}$ becomes

$$\begin{aligned}\frac{\text{d}}{\text{d}t}\sigma_{\mu\nu} &= i(\omega_\mu-\omega_\nu)\sigma_{\mu\nu}-ia_{\text{in}}^{\dagger}\left[\sigma_{\text{t}},\sigma_{\mu\nu}\right]-\frac{1}{2}\sigma_{\text{t}}^{\dagger}\left[\sigma_{\text{t}},\sigma_{\mu\nu}\right]+i\left[\sigma_{\text{t}}^{\dagger},\sigma_{\mu\nu}\right]a_{\text{in}}+\frac{1}{2}\left[\sigma_{\text{t}}^{\dagger},\sigma_{\mu\nu}\right]\sigma_{\text{t}}\\ &= i\omega_{\mu\nu}\sigma_{\mu\nu}+ia_{\text{in}}^{\dagger}\left[\sigma_{\mu\nu},\sigma_{\text{t}}\right]-i\left[\sigma_{\mu\nu},\sigma_{\text{t}}^{\dagger}\right]a_{\text{in}}-\frac{1}{2}\sigma_{\mu\nu}\sigma_{\text{t}}^{\dagger}\sigma_{\text{t}}-\frac{1}{2}\sigma_{\text{t}}^{\dagger}\sigma_{\text{t}}\sigma_{\mu\nu}+\sigma_{\text{t}}^{\dagger}\sigma_{\mu\nu}\sigma_{\text{t}}\\ &= i\omega_{\mu\nu}\sigma_{\mu\nu}-\xi_{\mu\nu}-i\zeta_{\mu\nu}a_{\text{in}}(t)+ia_{\text{in}}^{\dagger}(t)\zeta_{\nu\mu}^{\dagger}\end{aligned} \tag{B.14}$$

with

$$\xi_{\mu\nu}=\frac{1}{2}\sigma_{\mu\nu}\sigma_{\text{t}}^{\dagger}\sigma_{\text{t}}+\frac{1}{2}\sigma_{\text{t}}^{\dagger}\sigma_{\text{t}}\sigma_{\mu\nu}-\sigma_{\text{t}}^{\dagger}\sigma_{\mu\nu}\sigma_{\text{t}}, \tag{B.15}$$

$$\zeta_{\mu\nu}=\left[\sigma_{\mu\nu},\sigma_{\text{t}}^{\dagger}\right]. \tag{B.16}$$

The total solution of equation (B.14) contains a steady-state and a linear-response part

$$\left\langle\sigma_{\mu\nu}\right\rangle=\left\langle\sigma_{\mu\nu}\right\rangle_{\text{S}}+\left\langle\sigma_{\mu\nu}\right\rangle_{\text{L}}\text{e}^{\text{i}(\omega_{\text{d}}-\omega_{\text{p}})t}, \tag{B.17}$$

where ω_{p} is the probe frequency. The steady-state component $\left\langle\sigma_{\mu\nu}\right\rangle_{\text{S}}$ of equation (B.17) is calculated from equation (B.14) with the probe turned off ($\left\langle a_{\text{in}}\right\rangle=0$), i.e., by solving

$$i\omega_{\mu\nu}\left\langle\sigma_{\mu\nu}\right\rangle_{\text{S}}-\sum_{\mu'\,\nu'}\xi_{\mu\nu,\mu'\nu'}\left\langle\sigma_{\mu'\nu'}\right\rangle_{\text{S}}=0, \tag{B.18}$$

where $\xi_{\mu\nu,\mu'\nu'}=\left\langle\mu'\left|\xi_{\mu,\nu}\right|\nu'\right\rangle$, and applying the condition $\sum_{\mu}\left\langle\sigma_{\mu\mu}\right\rangle_{\text{S}}=1$. Together with the linear-response part $\left\langle\sigma_{\mu\nu}\right\rangle_{\text{L}}\text{e}^{\text{i}(\omega_{\text{d}}-\omega_{\text{p}})t}$, this gives

$$\begin{aligned}\frac{\text{d}}{\text{d}t}\left(\left\langle\sigma_{\mu\nu}\right\rangle_{\text{S}}+\left\langle\sigma_{\mu\nu}\right\rangle_{\text{L}}\text{e}^{\text{i}(\omega_{\text{d}}-\omega_{\text{p}})t}\right) &= i\omega_{\mu\nu}\left(\left\langle\sigma_{\mu\nu}\right\rangle_{\text{S}}+\left\langle\sigma_{\mu\nu}\right\rangle_{\text{L}}\text{e}^{\text{i}(\omega_{\text{d}}-\omega_{\text{p}})t}\right)\\ &\quad-\sum_{\mu'\nu'}\xi_{\mu\nu,\mu'\nu'}\left(\left\langle\sigma_{\mu'\nu'}\right\rangle_{\text{S}}+\left\langle\sigma_{\mu'\nu'}\right\rangle_{\text{L}}\text{e}^{\text{i}(\omega_{\text{d}}-\omega_{\text{p}})t}\right)\\ &\quad-i\sum_{\mu'\nu'}\zeta_{\mu\nu,\mu'\nu'}\left(\left\langle\sigma_{\mu'\nu'}\right\rangle_{\text{S}}+\left\langle\sigma_{\mu'\nu'}\right\rangle_{\text{L}}\text{e}^{\text{i}(\omega_{\text{d}}-\omega_{\text{p}})t}\right)F\text{e}^{\text{i}(\omega_{\text{d}}-\omega_{\text{p}})t}\\ &\quad+i\sum_{\mu'\nu'}\zeta_{\nu\mu,\nu'\mu'}\left(\left\langle\sigma_{\nu'\mu'}\right\rangle_{\text{S}}+\left\langle\sigma_{\nu'\mu'}\right\rangle_{\text{L}}\text{e}^{\text{i}(\omega_{\text{d}}-\omega_{\text{p}})t}\right)F\text{e}^{-\text{i}(\omega_{\text{d}}-\omega_{\text{p}})t},\end{aligned} \tag{B.19}$$

with $\zeta_{\mu\nu,\mu'\nu'} = \langle \mu' | \zeta_{\mu\nu} | \nu' \rangle$ and F the amplitude of the weak probe ($|F|^2$ is the number of incoming probe photons per second). Now we use $\frac{\mathrm{d}}{\mathrm{d}t}\langle\sigma_{\mu\nu}\rangle_{\mathrm{S}} = 0$, $\frac{\mathrm{d}}{\mathrm{d}t}\langle\sigma_{\mu\nu}\rangle_{\mathrm{L}} = \left(\omega_{\mathrm{d}} - \omega_{\mathrm{p}}\right)\langle\sigma_{\mu\nu}\rangle_{\mathrm{L}}$, $i\omega_{\mu\nu}\langle\sigma_{\mu\nu}\rangle_{\mathrm{S}} = \sum_{\mu'\nu'}\xi_{\mu\nu,\mu'\nu'}\langle\sigma_{\mu'\nu'}\rangle_{\mathrm{S}}$, $F \times \langle\sigma_{\mu'\nu'}\rangle_{\mathrm{L}} \ll 1$, and neglect fast rotating terms. We then find

$$i\left(\omega_{\mu\nu} - \omega_{\mathrm{d}} + \omega_{\mathrm{p}}\right)\langle\sigma_{\mu\nu}\rangle_{\mathrm{L}} - \sum_{\mu'\nu'}\xi_{\mu\nu,\mu'\nu'}\langle\sigma_{\mu\nu}\rangle_{\mathrm{L}}\mathrm{e}^{\mathrm{i}(\omega_{\mathrm{d}}-\omega_{\mathrm{p}})t} = iF \times \sum_{\mu'\nu'}\zeta_{\mu\nu,\mu'\nu'}\langle\sigma_{\mu'\nu'}\rangle_{\mathrm{S}}. \tag{B.20}$$

The reflection coefficient is defined by

$$r = \frac{\langle a_{\mathrm{out}}\rangle}{\langle a_{\mathrm{in}}\rangle}, \tag{B.21}$$

with

$$\langle a_{\mathrm{in}}\rangle = F\mathrm{e}^{\mathrm{i}(\omega_{\mathrm{d}}-\omega_{\mathrm{p}})t} \tag{B.22}$$

$$\langle a_{\mathrm{out}}\rangle = \langle a_{\mathrm{in}}\rangle - i\langle\sigma_{\mathrm{t}}\rangle = \left(F - i\sum_{\mu\nu}\sigma_{\mathrm{t},\mu\nu}\langle\sigma_{\mu\nu}\rangle_{\mathrm{L}}\right)\mathrm{e}^{\mathrm{i}(\omega_{\mathrm{d}}-\omega_{\mathrm{p}})t} \tag{B.23}$$

and $\sigma_{\mathrm{t},\mu\nu} = \langle\mu|\sigma_{\mathrm{t}}|\nu\rangle$. By solving equation (B.20) we can calculate the reflection coefficients for the two- and three-level systems in sections 3 and 4.

ORCID iDs

Emely Wiegand https://orcid.org/0000-0002-7881-4122
Anton Frisk Kockum https://orcid.org/0000-0002-2534-3021

References

[1] Clerk A A, Devoret M H, Girvin S M, Marquardt F and Schoelkopf R J 2010 Introduction to quantum noise, measurement, and amplification *Rev. Mod. Phys.* **82** 1155
[2] Aumentado J 2020 Superconducting parametric amplifiers: the state of the art in Josephson parametric amplifiers *IEEE Microwave* **21** 45
[3] Haus H A and Mullen J A 1962 Quantum noise in linear amplifiers *Phys. Rev.* **128** 2407
[4] Caves C M 1982 Quantum limits on noise in linear amplifiers *Phys. Rev.* D **26** 1817
[5] Leuchs G and Sondermann M 2013 Light–matter interaction in free space *J. Mod. Opt.* **60** 36
[6] Gerhardt I, Wrigge G, Bushev P, Zumofen G, Agio M, Pfab R and Sandoghdar V 2007 Strong extinction of a laser beam by a single molecule *Phys. Rev. Lett.* **98** 033601
[7] Vamivakas A N, Atatüre M, Dreiser J, Yilmaz S T, Badolato A, Swan A K, Goldberg B B, Imamoğlu A and Ünlü M S 2007 Strong extinction of a far-field laser beam by a single quantum dot *Nano Lett.* **7** 2892
[8] Wrigge G, Gerhardt I, Hwang J, Zumofen G and Sandoghdar V 2008 Efficient coupling of photons to a single molecule and the observation of its resonance fluorescence *Nat. Phys.* **4** 60
[9] Tey M K, Chen Z, Aljunid S A, Chng B, Huber F, Maslennikov G and Kurtsiefer C 2008 Strong interaction between light and a single trapped atom without the need for a cavity *Nat. Phys.* **4** 924
[10] Hwang J, Pototschnig M, Lettow R, Zumofen G, Renn A, Götzinger S and Sandoghdar V 2009 A single-molecule optical transistor *Nature* **460** 76
[11] Leong V, Seidler M A, Steiner M, Cerè A and Kurtsiefer C 2016 Time-resolved scattering of a single photon by a single atom *Nat. Commun.* **7** 13716
[12] Roy D, Wilson C M and Firstenberg O 2017 Colloquium: strongly interacting photons in one-dimensional continuum *Rev. Mod. Phys.* **89** 021001
[13] Gu X, Kockum A F, Miranowicz A, Liu Y-x and Nori F 2017 Microwave photonics with superconducting quantum circuits *Phys. Rep.* **718–719** 1
[14] You J Q and Nori F 2011 Atomic physics and quantum optics using superconducting circuits *Nature* **474** 589
[15] Kockum A F and Nori F 2019 *Fundamentals and Frontiers of the Josephson Effect* ed F Tafuri (Berlin: Springer) pp 703–41
[16] Blais A, Grimsmo A L, Girvin S M and Wallraff A 2020 Circuit quantum electrodynamics (arXiv:2005.12667)
[17] Astafiev O, Inomata K, Niskanen A O, Yamamoto T, Pashkin Y A, Nakamura Y and Tsai J S 2007 Single artificial-atom lasing *Nature* **449** 588
[18] Ashhab S, Johansson J R, Zagoskin A M and Nori F 2009 Single-artificial-atom lasing using a voltage-biased superconducting charge qubit *New J. Phys.* **11** 023030
[19] You J Q, Liu Y-x, Sun C P and Nori F 2007 Persistent single-photon production by tunable on-chip micromaser with a superconducting quantum circuit *Phys. Rev.* B **75** 104516
[20] Marthaler M, Utsumi Y, Golubev D S, Shnirman A and Schön G 2011 Lasing without inversion in circuit quantum electrodynamics *Phys. Rev. Lett.* **107** 093901
[21] Kjaergaard M, Schwartz M E, Braumüller J, Krantz P, Wang J I-J, Gustavsson S and Oliver W D 2020 Superconducting qubits: current state of play *Annu. Rev. Condens. Matter Phys.* **11** 369
[22] Blais A, Huang R-S, Wallraff A, Girvin S M and Schoelkopf R J 2004 Cavity quantum electrodynamics for superconducting electrical circuits: an architecture for quantum computation *Phys. Rev.* A **69** 062320
[23] Wallraff A, Schuster D I, Blais A, Frunzio L, Huang R S, Majer J, Kumar S, Girvin S M and Schoelkopf R J 2004 Strong coupling of a single photon to a superconducting qubit using circuit quantum electrodynamics *Nature* **431** 162

[24] Astafiev O, Zagoskin A M, Abdumalikov A A, Pashkin Y A, Yamamoto T, Inomata K, Nakamura Y and Tsai J S 2010 Resonance fluorescence of a single artificial atom *Science* **327** 840
[25] Paik H *et al* 2011 Observation of high coherence in Josephson junction qubits measured in a three-dimensional circuit QED architecture *Phys. Rev. Lett.* **107** 240501
[26] Devoret M H, Girvin S and Schoelkopf R 2007 Circuit-QED: how strong can the coupling between a Josephson junction atom and a transmission line resonator be? *Ann. Phys.* **16** 767
[27] Bourassa J, Gambetta J M, Abdumalikov A A, Astafiev O, Nakamura Y and Blais A 2009 Ultrastrong coupling regime of cavity QED with phase-biased flux qubits *Phys. Rev.* A **80** 032109
[28] Niemczyk T *et al* 2010 Circuit quantum electrodynamics in the ultrastrong-coupling regime *Nat. Phys.* **6** 772
[29] Forn-Díaz P, García-Ripoll J J, Peropadre B, Orgiazzi J-L, Yurtalan M A, Belyansky R, Wilson C M and Lupascu A 2017 Ultrastrong coupling of a single artificial atom to an electromagnetic continuum in the nonperturbative regime *Nat. Phys.* **13** 39
[30] Yoshihara F, Fuse T, Ashhab S, Kakuyanagi K, Saito S and Semba K 2017 Superconducting qubit-oscillator circuit beyond the ultrastrong-coupling regime *Nat. Phys.* **13** 44
[31] Kockum A F, Miranowicz A, De Liberato S, Savasta S and Nori F 2019 Ultrastrong coupling between light and matter *Nat. Rev. Phys.* **1** 19
[32] Forn-Díaz P, Lamata L, Rico E, Kono J and Solano E 2019 Ultrastrong coupling regimes of light–matter interaction *Rev. Mod. Phys.* **91** 025005
[33] Wen P Y, Kockum A F, Ian H, Chen J C, Nori F and Hoi I-C 2018 Reflective amplification without population inversion from a strongly driven superconducting qubit *Phys. Rev. Lett.* **120** 063603
[34] Wu F Y, Ezekiel S, Ducloy M and Mollow B R 1977 Observation of amplification in a strongly driven two-level atomic system at optical frequencies *Phys. Rev. Lett.* **38** 1077
[35] Xu X, Sun B, Berman P R, Steel D G, Bracker A S, Gammon D and Sham L J 2007 Coherent optical spectroscopy of a strongly driven quantum dot *Science* **317** 929
[36] Astafiev O V, Abdumalikov A A, Zagoskin A M, Pashkin Y A, Nakamura Y and Tsai J S 2010 Ultimate on-chip quantum amplifier *Phys. Rev. Lett.* **104** 183603
[37] Hoi I-C, Wilson C M, Johansson G, Palomaki T, Peropadre B and Delsing P 2011 Demonstration of a single-photon router in the microwave regime *Phys. Rev. Lett.* **107** 073601
[38] Hoi I-C, Palomaki T, Lindkvist J, Johansson G, Delsing P and Wilson C M 2012 Generation of nonclassical microwave states using an artificial atom in 1D open space *Phys. Rev. Lett.* **108** 263601
[39] van Loo A F, Fedorov A, Lalumière K, Sanders B C, Blais A and Wallraff A 2013 Photon-mediated interactions between distant artificial atoms *Science* **342** 1494
[40] Koshino K, Terai H, Inomata K, Yamamoto T, Qiu W, Wang Z and Nakamura Y 2013 Observation of the three-state dressed states in circuit quantum electrodynamics *Phys. Rev. Lett.* **110** 263601
[41] Hoi I-C, Wilson C M, Johansson G, Lindkvist J, Peropadre B, Palomaki T and Delsing P 2013 Microwave quantum optics with an artificial atom in one-dimensional open space *New J. Phys.* **15** 025011
[42] Hoi I-C *et al* 2013 Giant cross-Kerr effect for propagating microwaves induced by an artificial atom *Phys. Rev. Lett.* **111** 053601
[43] Liu Y and Houck A A 2017 Quantum electrodynamics near a photonic bandgap *Nat. Phys.* **13** 48
[44] Mirhosseini M, Kim E, Ferreira V S, Kalaee M, Sipahigil A, Keller A J and Painter O 2018 Superconducting metamaterials for waveguide quantum electrodynamics *Nat. Commun.* **9** 3706
[45] Sundaresan N M, Lundgren R, Zhu G, Gorshkov A V and Houck A A 2019 Interacting qubit-photon bound states with superconducting circuits *Phys. Rev.* X **9** 011021
[46] Wen P Y *et al* 2019 Large collective lamb shift of two distant superconducting artificial atoms *Phys. Rev. Lett.* **123** 233602
[47] Mirhosseini M, Kim E, Zhang X, Sipahigil A, Dieterle P B, Keller A J, Asenjo-Garcia A, Chang D E and Painter O 2019 Cavity quantum electrodynamics with atom-like mirrors *Nature* **569** 692
[48] Kannan B *et al* 2020 Waveguide quantum electrodynamics with superconducting artificial giant atoms *Nature* **583** 775
[49] Vadiraj A M, Ask A, McConkey T G, Nsanzineza I, Sandbo Chang C W, Kockum A F and Wilson C M 2020 Engineering the level structure of a giant artificial atom in waveguide quantum electrodynamics (arXiv:2003.14167)
[50] Johansson J R, Johansson G, Wilson C M and Nori F 2009 Dynamical Casimir effect in a superconducting coplanar waveguide *Phys. Rev. Lett.* **103** 147003
[51] Wilson C M, Johansson G, Pourkabirian A, Simoen M, Johansson J R, Duty T, Nori F and Delsing P 2011 Observation of the dynamical Casimir effect in a superconducting circuit *Nature* **479** 376
[52] Hoi I-C, Kockum A F, Tornberg L, Pourkabirian A, Johansson G, Delsing P and Wilson C M 2015 Probing the quantum vacuum with an artificial atom in front of a mirror *Nat. Phys.* **11** 1045
[53] Eschner J, Raab C, Schmidt-Kaler F and Blatt R 2001 Light interference from single atoms and their mirror images *Nature* **413** 495
[54] Wilson M A, Bushev P, Eschner J, Schmidt-Kaler F, Becher C, Blatt R and Dorner U 2003 Vacuum-field level shifts in a single trapped ion mediated by a single distant mirror *Phys. Rev. Lett.* **91** 213602
[55] Dubin F, Rotter D, Mukherjee M, Russo C, Eschner J and Blatt R 2007 Photon correlation versus interference of single-atom fluorescence in a half-cavity *Phys. Rev. Lett.* **98** 183003
[56] Lu Y *et al* 2021 Characterizing decoherence rates of a superconducting qubit by direct microwave scattering *npj Quantum Inf.* **7** 35
[57] Scigliuzzo M, Bengtsson A, Besse J-C, Wallraff A, Delsing P and Gasparinetti S 2020 Primary thermometry of propagating microwaves in the quantum regime *Phys. Rev.* X **10** 041054
[58] Meschede D, Jhe W and Hinds E A 1990 Radiative properties of atoms near a conducting plane: an old problem in a new light *Phys. Rev.* A **41** 1587
[59] Dorner U and Zoller P 2002 Laser-driven atoms in half-cavities *Phys. Rev.* A **66** 023816
[60] Beige A, Pachos J and Walther H 2002 Spontaneous emission of an atom in front of a mirror *Phys. Rev.* A **66** 063801
[61] Dong H, Gong Z R, Ian H, Zhou L and Sun C P 2009 Intrinsic cavity QED and emergent quasinormal modes for a single photon *Phys. Rev.* A **79** 063847
[62] Koshino K and Nakamura Y 2012 Control of the radiative level shift and linewidth of a superconducting artificial atom through a variable boundary condition *New J. Phys.* **14** 043005
[63] Wang Y, Minár J, Hétet G and Scarani V 2012 Quantum memory with a single two-level atom in a half cavity *Phys. Rev.* A **85** 013823

[64] Tufarelli T, Ciccarello F and Kim M S 2013 Dynamics of spontaneous emission in a single-end photonic waveguide *Phys. Rev.* A **87** 013820
[65] Fang Y-L L and Baranger H U 2015 Waveguide QED: power spectra and correlations of two photons scattered off multiple distant qubits and a mirror *Phys. Rev.* A **91** 053845
[66] Shi T, Chang D E and Cirac J I 2015 Multiphoton-scattering theory and generalized master equations *Phys. Rev.* A **92** 053834
[67] Pichler H and Zoller P 2016 Photonic circuits with time delays and quantum feedback *Phys. Rev. Lett.* **116** 093601
[68] Pichler H, Choi S, Zoller P and Lukin M D 2017 Universal photonic quantum computation via time-delayed feedback *Proc. Natl Acad. Sci. USA* **114** 11362
[69] Wiegand E, Rousseaux B and Johansson G 2020 Semiclassical analysis of dark-state transient dynamics in waveguide circuit QED *Phys. Rev.* A **101** 033801
[70] Wiegand E, Rousseaux B and Johansson G 2021 Transmon in a semi-infinite high-impedance transmission line: appearance of cavity modes and Rabi oscillations *Phys. Rev. Research* **3** 023003
[71] Sargent M, Scully M O and Lamb W E 1974 *Laser Physics* (Reading, MA: Addison-Wesley Developers Press)
[72] Silfvast W T 1996 *Laser Fundamentals* (Cambridge: Cambridge University Press)
[73] Mompart J and Corbalán R 2000 Lasing without inversion *J. Opt. B: Quantum Semiclass. Opt.* **2** R7
[74] Haroche S and Hartmann F 1972 Theory of saturated-absorption line shapes *Phys. Rev.* A **6** 1280
[75] Mollow B R 1969 Power spectrum of light scattered by two-level systems *Phys. Rev.* **188** 1969
[76] Abdumalikov A A, Astafiev O V, Pashkin Y A, Nakamura Y and Tsai J S 2011 Dynamics of coherent and incoherent emission from an artificial atom in a 1D space *Phys. Rev. Lett.* **107** 043604
[77] Mollow B R 1972 Stimulated emission and absorption near resonance for driven systems *Phys. Rev.* A **5** 2217
[78] Friedmann H and Wilson-Gordon A D 1987 Dispersion profiles of the absorptive response of a two-level system interacting with two intense fields *Phys. Rev.* A **36** 1333
[79] Kockum A F 2021 *International Symposium on Mathematics, Quantum Theory, and Cryptography* (*Mathematics for Industry*) vol 33 (Berlin: Springer) pp 125–46
[80] Kockum A F, Delsing P and Johansson G 2014 Designing frequency-dependent relaxation rates and Lamb shifts for a giant artificial atom *Phys. Rev.* A **90** 013837
[81] Gustafsson M V, Aref T, Kockum A F, Ekström M K, Johansson G and Delsing P 2014 Propagating phonons coupled to an artificial atom *Science* **346** 207
[82] Guo L, Grimsmo A L, Kockum A F, Pletyukhov M and Johansson G 2017 Giant acoustic atom: a single quantum system with a deterministic time delay *Phys. Rev.* A **95** 053821
[83] Manenti R, Kockum A F, Patterson A, Behrle T, Rahamim J, Tancredi G, Nori F and Leek P J 2017 Circuit quantum acoustodynamics with surface acoustic waves *Nat. Commun.* **8** 975
[84] Kockum A F, Johansson G and Nori F 2018 Decoherence-free interaction between giant atoms in waveguide quantum electrodynamics *Phys. Rev. Lett.* **120** 140404
[85] Karg T M, Gouraud B, Treutlein P and Hammerer K 2019 Remote Hamiltonian interactions mediated by light *Phys. Rev.* A **99** 063829
[86] Ask A, Ekström M, Delsing P and Johansson G 2019 Cavity-free vacuum-Rabi splitting in circuit quantum acoustodynamics *Phys. Rev.* A **99** 013840
[87] González-Tudela A, Sánchez Muñoz C and Cirac J I 2019 Engineering and harnessing giant atoms in high-dimensional baths: a proposal for implementation with cold atoms *Phys. Rev. Lett.* **122** 203603
[88] Guimond P-O, Vermersch B, Juan M L, Sharafiev A, Kirchmair G and Zoller P 2020 A unidirectional on-chip photonic interface for superconducting circuits *npj Quantum Inf.* **6** 32
[89] Guo L, Kockum A F, Marquardt F and Johansson G 2020 Oscillating bound states for a giant atom *Phys. Rev. Res.* **2** 043014
[90] Wang X, Liu T, Kockum A F, Li H-R and Nori F 2020 Tunable chiral bound states with giant atoms (arXiv:2008.13560)
[91] Ask A, Fang Y-L L and Kockum A F 2020 Synthesizing electromagnetically induced transparency without a control field in waveguide QED using small and giant atoms (arXiv:2011.15077)
[92] Koch J *et al* 2007 Charge-insensitive qubit design derived from the Cooper pair box *Phys. Rev.* A **76** 042319
[93] Sandberg M, Wilson C M, Persson F, Bauch T, Johansson G, Shumeiko V, Duty T and Delsing P 2008 Tuning the field in a microwave resonator faster than the photon lifetime *Appl. Phys. Lett.* **92** 203501
[94] Sathyamoorthy S R, Tornberg L, Kockum A F, Baragiola B Q, Combes J, Wilson C M, Stace T M and Johansson G 2014 Quantum nondemolition detection of a propagating microwave photon *Phys. Rev. Lett.* **112** 093601